Acta Crystallographica Section D
Biological Crystallography
ISSN 0907-4449

Critical catalytic functional groups in the mechanism of aspartate-β-semialdehyde dehydrogenase

Julio Blanco, Roger A. Moore,‡ Christopher R. Faehnle and Ronald E. Viola*

Department of Chemistry, University of Toledo, Toledo, Ohio 43606, USA

‡ Present address: Laboratory of Persistent Viral Diseases, Rocky Mountain Laboratories, NIAID, NIH, Hamilton, MT 59840, USA.

Correspondence e-mail: ron.viola@utoledo.edu

Received 5 August 2004
Accepted 12 August 2004

PDB References: C136S ASADH, 1pqp, r1pqpsf; H277N ASADH, 1pqu, r1pqusf.

Aspartate-β-semialdehyde dehydrogenase (ASADH) catalyzes the reductive dephosphorylation of β-aspartyl phosphate to L-aspartate-β-semialdehyde in the aspartate biosynthetic pathway. This pathway is not found in humans or other eukaryotic organisms, yet is required for the production of threonine, isoleucine, methionine and lysine in most microorganisms. The mechanism of this enzyme has been examined through the structures of two active-site mutants of ASADH from *Haemophilus influenzae*. Replacement of the enzyme active-site cysteine with serine (C136S) leads to a dramatic loss of catalytic activity caused by the expected decrease in nucleophilicity, but also by a change in the orientation of the serine hydroxyl group relative to the cysteine thiolate. In contrast, in the H277N active-site mutant the introduced amide is oriented in virtually the same position as that of the histidine imidazole ring. However, a shift in the position of the bound reaction intermediate to accommodate this shorter asparagine side chain, coupled with the inability of this introduced amide to serve as a proton acceptor, results in a 100-fold decrease in the catalytic efficiency of H277N relative to the native enzyme. These mutant enzymes have the same overall fold and high structural identity to native ASADH. However, small perturbations in the positioning of essential catalytic groups or reactive intermediates have dramatic effects on catalytic efficiency.

1. Introduction

Aspartate-β-semialdehyde dehydrogenase (ASADH; EC 1.2.1.11) catalyzes the reductive dephosphorylation of β-aspartyl phosphate (βAP) to L-aspartate-β-semialdehyde (ASA) (Fig. 1) in the aspartate biosynthetic pathway (Cohen, 1983; Viola, 2001). At this key branch point, the product ASA is either further reduced to homoserine and then converted to threonine, isoleucine and methionine or is condensed with pyruvate to produce diaminopimelic acid, a cross-linking component in the peptidoglycan layer of bacterial cell walls and a direct precursor of lysine (Patte, 1983). Since this pathway is not found in humans or other eukaryotic organisms, specific inhibition of key enzymes can be quite selective

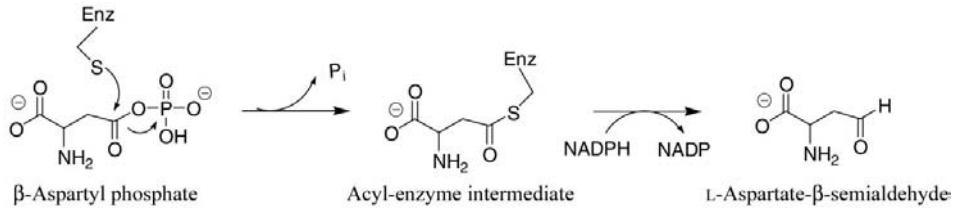

Figure 1
The reductive dephosphorylation of β-aspartyl phosphate to L-aspartate-β-semialdehyde. This reaction proceeds through a covalent acyl-enzyme intermediate catalyzed by ASADH.

for the aspartate pathway, making ASADH a reasonable target for the development of new antimicrobial compounds. Perturbations of the *asd* gene encoding ASADH can be lethal to microorganisms, as has been demonstrated for *Legionella pneumophia* and *Salmonella typhimurium* (Galan *et al.*, 1990; Harb & Kwaik, 1998; Kang *et al.*, 2002; Nakayama *et al.*, 1988). Consequently, there is continued interest in the development of effective microbial ASADH inhibitors (Cox *et al.*, 2000, 2001).

Structures of ASADH from the Gram-negative microorganisms *Escherichia coli* (Hadfield *et al.*, 1999, 2001), *Vibrio cholerae* (Blanco, Moore, Kalabeeswaran *et al.*, 2003) and *Haemophilus influenzae* (Blanco, Moore & Viola, 2003) have been solved as the apoenzyme, as a ternary complex with NADP and the active-site inhibitor *S*-methyl-L-cysteine sulfoxide (SMCS), and also with the substrate ASA covalently bound to the active site. Recently completed studies of several mutants have established the identity of the substrate-binding groups in ASADH (Blanco *et al.*, 2004). Each structure has helped to clarify the roles of those active-site amino acids previously identified by site-directed mutagenesis (Ouyang & Viola, 1995) and has further expanded the set of catalytically relevant amino acids. The catalytic mechanism of ASADH is similar to that of glyceraldehyde-3-phosphate dehydrogenase (GAPDH). Both ASADH and GAPDH utilize a cysteine nucleophile and an adjacent histidine functioning together as an active-site dyad to initiate catalysis (Biellmann *et al.*, 1980; Holland & Westhead, 1973). Chemical modification (Harris & Waters, 1976) and X-ray structural studies (Krimsky & Racker, 1955; Moras *et al.*, 1975) on GAPDH have implicated a cysteine sulfhydryl group as the active-site nucleophile. These studies support the formation of a thioester intermediate in the catalytic cycle of GAPDH (Krimsky & Racker, 1955; Yun *et al.*, 2000). Here, we report the kinetic and structural characterization of mutations of the critical active-site catalytic dyad of ASADH from *H. influenzae*, an infectious microorganism whose only natural host is human and is further distinguished as the first free-living organism to have its complete genome sequenced (Fleischmann *et al.*, 1995).

2. Experimental procedures

2.1. Preparation and purification of ASADH mutants

The *asd* gene from *H. influenzae* that encodes ASADH (*hi*ASADH, Swiss-Prot P44801) was subcloned into a pET expression system (pET41a/*asd*) and overexpressed as described previously (Moore *et al.*, 2002). Mutations were created with this vector as the template using the QuikChange protocol (Strategene). For the low-activity mutants, the *asd*-containing plasmid was transformed into a Δ*asd E. coli* cell line (Hfr3000 U482) to eliminate trace interference from genomic ASADH. These mutants of *H. influenzae* ASADH were purified to homogeneity by following the same protocol as used for native enzyme (Moore *et al.*, 2002), concentrated by centrifugal ultrafiltration (Millipore) to 15 mg ml^{-1} and dialyzed against 10 m*M* sodium HEPES pH 7.0 containing 1 m*M* EDTA and 1 m*M* DTT.

Table 1
Data-collection statistics for *H. influenzae* ASADH catalytic mutants.

Values in parentheses are for the highest resolution shell.

Data set	C136S–ASA	C136S–ASA–P_i	H277N–NADP–SMCS
Wavelength (Å)	1.00	1.00	1.00
Space group	$P2_12_12$	$P2_12_12$	$P2_1$
Unit-cell parameters			
a (Å)	114.0	113.9	72.9
b (Å)	55.0	55.1	76.6
c (Å)	57.6	57.8	134.1
β (°)			92.6
Resolution (Å)	2.00	2.06	1.92
No. observations			
Measured	553012	286785	732634
Unique	30016	27514	99660
Completeness (%)	95.1 (96.9)	94.5 (85.8)	89.0 (90.7)
R_{sym}† (%)	8.3	4.9	8.0
Average $\langle I/\sigma(I)\rangle$	19.6	29.8	10.7

† $R_{sym} = \sum_{hkl}\sum_i |I_{hkl,i} - \langle I_{hkl}\rangle| / \sum_{hkl,i} I_{hkl,i}$, where $I_{hkl,i}$ is the intensity of an individual measurement of the reflection with Miller indices h, k and l and $\langle I_{hkl}\rangle$ is the mean intensity of that reflection.

2.2. Crystallization of the ASADH mutants

Initial crystallization conditions were obtained by hanging-drop vapor diffusion using the PEG/Ion Screen (Hampton Research). After further optimization, crystals were grown at 293 K in 1:1 mixtures of enzyme and precipitant solution (24–28% PEG 3350, 0.2 *M* ammonium acetate and 0.1 *M* Tris–HCl pH 8.5).

2.3. Formation of the enzyme–substrate complexes

Apoenzyme crystals of C136S ASADH were complexed by soaking with either ASA or with ASA and phosphate. A suitable crystal was introduced into artificial mother liquor (26% PEG 3350, 0.2 *M* ammonium acetate and 0.1 *M* Tris–HCl pH 8.5). ASA was then added to the mother liquor from a stock concentration of 100 m*M* to a final concentration of 2 m*M*. In the case where phosphate was introduced, the

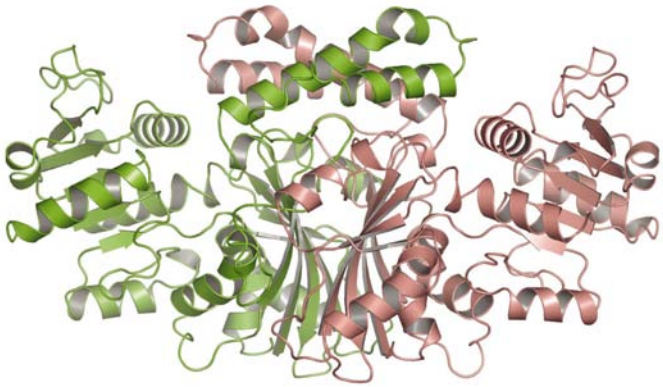

Figure 2
Ribbon drawing of the dimeric structure of *hi*ASADH C136S. The two monomers are represented in different colors.

crystals were soaked in the presence of 100 m*M* sodium phosphate for 1 h before harvesting. A harvesting solution (26% PEG 3350, 0.2 *M* ammonium acetate, 2 m*M* ASA with or without 100 m*M* phosphate and 0.1 *M* Tris–HCl pH 8.5 containing 20% glycerol) was introduced stepwise over approximately 1 h, followed by flash-freezing of the crystals.

In the case of the H277N mutant, suitable crystals for data collection were obtained in the presence of 5 m*M* each of NADP and SMCS and were grown at 293 K from 1:1 mixtures of enzyme solution (15 mg ml^{-1}) and precipitant (22% PEG 3350, 0.2 *M* ammonium acetate and 0.1 *M* sodium cacodylate, pH 6.5).

2.4. Data collection and processing

Diffraction data from each of the *hi*ASADH catalytic mutants were collected at the Structural Biology Center (SBC) beamline at APS using an SBC-2 CCD X-ray detector. The images were processed and scaled using the program *HKL*2000 (Otwinowski & Minor, 1997). Data-collection statistics for each of these data sets are summarized in Table 1.

2.5. Structure solution and refinement

Data sets for the C136S mutant belong to the $P2_12_12$ space group and give a monomer in the asymmetric unit. For the H277N mutant, the data were indexed and processed in space group $P2_1$, giving two dimers per asymmetric unit (Table 1). The structures were solved by molecular replacement using the *H. influenzae* apo-ASADH (PDB code 1nwc) structure as the search model. The *CNS* package was used for the rotation and translation searches (Brünger *et al.*, 1998). Rigid-body refinement led to an *R* factor of approximately 30% at a resolution between 20.0 and 3.0 Å. Simulated-annealing refinement was then applied to the coordinate file obtained from the rigid-body refinement, improving the *R* factor to 25%. Model building was applied using *XtalView* (McRee, 1999). Several iterations of refinement and model building improved the final structure; the refined coordinates were deposited with the PDB and assigned the entry code 1pqp.

In case of the H277N structure, a dimer from the same *H. influenzae* apo-ASADH structure was used as the model for molecular replacement. After the rotation and translation solution was found for the first molecule, a second translation search was performed after non-crystallographic symmetry had been applied to the coordinates of the first molecule, yielding a solution corresponding to the position of the second dimer. A rigid-body refinement applied to these coordinates improved the *R* factor to 34%. Simulated-annealing refinement at 2.5 Å was applied to the coordinate file obtained from the rigid-body refinement, improving the *R* factor to 28%. Several iterations of refinement, model building and addition of NADP and SMCS improved the final structure. The final refinement statistics for the structures are listed in Table 2. The refined coordinates for the H277N complex have been deposited with the PDB and assigned the entry code 1pqu.

Table 2
Structural refinement statistics for the catalytic mutants.

	C136S–ASA–P_i	C136S–ASA	H277N–NADP–SMCS
Refinement			
Resolution range (Å)	50–2.06	50–2.00	50–1.92
R_{cryst} (%)	22.7	23.5	18.3
R_{free} (%)	28.4	28.1	23.6
No. protein atoms	2755	2755	11281
No. non-protein atoms	13	8	192
No. water molecules	219	208	799
Stereochemistry			
R.m.s.d. for bond lengths (Å)	0.005	0.005	0.006
R.m.s.d. for bond angles (°)	1.3	1.3	1.3
Residues in the Ramachandran plot			
Most favored region (%)	88.0	90.3	89.3
Additional allowed regions (%)	11.0	8.8	10.0
Generously allowed regions (%)	1.0	1.0	0.7

2.6. Kinetic studies

Enzyme assays were performed on a Perkin–Elmer Lambda-1 spectrophotometer equipped with a thermostatted cell holder connected to a circulating water bath. The assay reaction monitors the oxidative phosphorylation of ASA in the non-physiological direction at 303 K in 200 m*M* sodium CHES pH 9.0 with 40 m*M* potassium phosphate and 1 m*M* NADP. Immediately after the addition of enzyme, the reaction was initiated by addition of ASA. Initial velocity measurements are based upon the rate of increasing NADPH absorbance at 340 nm (ε = 6.22 mM^{-1} cm^{-1}). Kinetic parameters for ASA, NADP and inorganic phosphate were determined by varying the concentration of one substrate at saturating levels (10–20 × K_m) of the fixed substrates and fitting the data to an enzyme-kinetics software package adapted from the programs of Cleland (1967). The k_{cat} values were calculated based on a subunit molecular weight of 40 kDa. Protein concentrations were determined by the method of Bradford, using a standard curve generated from known concentrations of bovine serum albumin (Bradford, 1976).

3. Results and discussion

Structural studies of enzyme–substrate, enzyme–intermediate and enzyme–product complexes serve to identify the set of functional groups that are in position to participate in the catalytic mechanism. However, definitive mechanistic conclusions must be derived from functional as well as structural studies that test these proposed roles. To provide this functional information for ASADH we have focused on the two key active-site amino acids, Cys136 and His277, each of which has been shown to play a critical catalytic role (Hadfield *et al.*, 1999; Karsten & Viola, 1992).

3.1. Function of the enzyme nucleophile

We recently determined the structure of a covalently bound hemithioacetal intermediate trapped in the active site of *hi*ASADH (Blanco, Moore & Viola, 2003). This structure supports the assignment of Cys136 as the enzyme nucleophile

Table 3
Kinetic parameters of the *H. influenzae* ASADH catalytic mutants.

		ASA		Phosphate		NADP	
Enzyme	k_{cat} (s^{-1})	K_m (m*M*)	k_{cat}/K_m (M^{-1} s^{-1})	K_m (m*M*)	k_{cat}/K_m (M^{-1} s^{-1})	K_m (m*M*)	k_{cat}/K_m (M^{-1} s^{-1})
Native	330 ± 17	0.20 ± 0.03	1.4×10^6	1.6 ± 0.2	2.1×10^5	0.20 ± 0.03	2.2×10^6
C136S	≤0.016†	—	—	—	—	—	—
H277N	3.2 ± 0.3	0.50 ± 0.10	6.4×10^3	2.7 ± 0.4	1.2×10^3	1.1 ± 0.2	3.0×10^3

† The low activity of this mutant precludes an accurate determination of its kinetic parameters.

and explicitly demonstrates for the first time the existence of a covalently bound intermediate in the mechanism of ASADH (Fig. 1). To verify the importance of Cys136 in the catalytic cycle of ASADH and to examine a substrate or product complex in a low-activity enzyme form, this catalytic residue was mutated to the less nucleophilic amino acid serine.

Crystals of C136S were grown and then soaked with ASA to form a binary (*hi*ASADH–ASA) complex. This same soaking experiment was conducted in the presence of phosphate to capture the inactive ternary (*hi*ASADH–ASA–P_i) complex with the two reaction products bound. Crystals of each of these complexes diffract to ∼2 Å and complete data sets were collected, modeled and refined for each complex as described in §2. The overall structure of this mutant (Fig. 2) is the same as that of the native enzyme, with the same dimer interface, coenzyme-binding domain fold and active-site cavity structure. Density that is consistent with the presence of a hydroxymethyl group was observed in the active site at position 136, confirming the replacement of the active-site cysteine with serine. The substrate ASA is bound non-covalently in the C136S mutant enzyme and well defined density is observed in the ternary *hi*ASADH–ASA–P_i complex both for ASA and for a single bound phosphate (Fig. 3). The density for ASA is less well defined in the binary complex, which is indicative of either a lower occupancy or some disorder of the bound substrate. This observation supports earlier kinetic studies, which showed that ASA binds with a greater affinity to the enzyme in the presence of bound phosphate (Karsten & Viola, 1991). Without the addition of the nucleotide coenzyme these *hi*ASADH structures are found in an open conformation, similar to the conformation that was observed for the *E. coli* apoenzyme (Hadfield *et al.*, 2001). A disordered loop (residues 40–54) that is normally involved in coenzyme binding was not modeled in these *hi*ASADH structures owing to a lack of convincing electron density. This same disorder is present in the native enzyme without bound NADP (Blanco, Moore & Viola, 2003). The failure of this loop to adopt a distinct well ordered conformation in the absence of NADP is indicative of the flexibility that is required for coenzyme binding.

3.2. Reorientation of the introduced serine

Except for this disordered loop, the overall structure of C136S does not deviate substantially from that of the native enzyme. Only minor changes were observed near the active site, despite the nearly complete loss of catalytic activity (Table 3). One significant change is an approximate 90° rotation of the hydroxyl side chain of the introduced Ser136 relative to the position occupied by the cysteine thiolate group in the native enzyme (Fig. 4*a*). This new orientation is stabilized by hydrogen bonding of the Ser136 hydroxyl group to the backbone carbonyl of Gly357, an interaction that is not observed in the native enzyme. Instead, the native enzyme stabilizes the thioester intermediate that is produced in the ASADH reaction through a water molecule hydrogen bonded to the backbone carbonyl of Gly357 (Blanco, Moore & Viola, 2003). Thus, the hydrogen bonding of this Gly357 carbonyl with Ser136 in the C136S mutant competes with the potential involvement of this carbonyl group in intermediate stabilization.

Importantly, occupancy in this new orientation would not allow the participation of His277 in the deprotonation of Ser136. Without assistance from a stronger adjacent base, the higher p*K* of the Ser136 hydroxyl group relative to the cysteine thiol precludes significant ionization in the pH range 7–10 where ASADH is optimally active and provides an additional explanation for the very low activity of this mutant (Table 3). Despite the presence of this less efficient nucleophile, the C136S mutant is still covalently inactivated by SMCS. This active-site-directed inactivation shows that this introduced side chain must be in the proper orientation to support catalysis at least some fraction of the time. However, significantly higher SMCS levels (50–100 m*M*) are required to effect the inactivation of this mutant when compared with the rapid inactivation of the native enzyme with much lower SMCS levels. Thus, replacement of a single atom in this enzyme, an oxygen for a sulfur in this critical active-site functional group, results in dramatically impaired catalysis.

3.3. Misalignment of the enzyme-bound substrate

The native enzyme binds and orients ASA such that the aldehydic carbon is positioned for attack by the Cys136 thiolate to form a covalently bound hemithioacetal (Blanco, Moore & Viola, 2003). The diminished ability of Ser136 to form this intermediate allows an opportunity to examine the position of the enzyme-bound substrate as it would be immediately prior to nucleophilic attack. Since the active-site architecture of the C136S mutant is nearly identical to that of the native enzyme, other than the misorientation of Ser136, the positions of bound ASA and phosphate in this structure are expected to be similar to those in the actual initial enzyme–substrate complex. However, an overlay of the C136S–ASA–P_i ternary complex with that of the covalently bound tetrahedral intermediate structure in the native enzyme (Fig. 4*b*) shows that the alignment of ASA within the active-site cavity must change after nucleophilic attack. In the substrate complex, the α-carboxyl group of ASA forms electrostatic interactions with both Arg270 and His277 and its α-amino group is also within hydrogen-bonding distance of

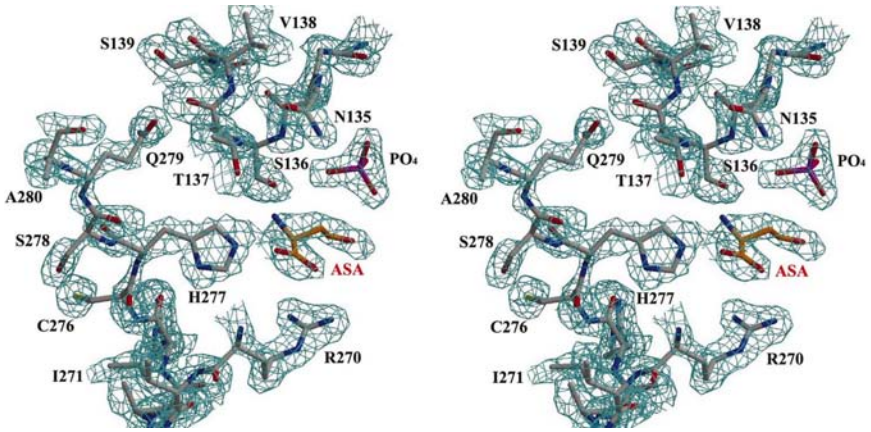

Figure 3
Representation of the $2F_o - F_c$ electron-density map of the active site of the *hi*ASADH C136S mutant with bound ASA and phosphate. The hydroxyl group of Ser136 is pointing away from the catalytic His277 that is proposed to deprotonate the active-site nucleophile. This figure, contoured at 1.3σ, was produced using *BOBSCRIPT* and *RASTER3D*.

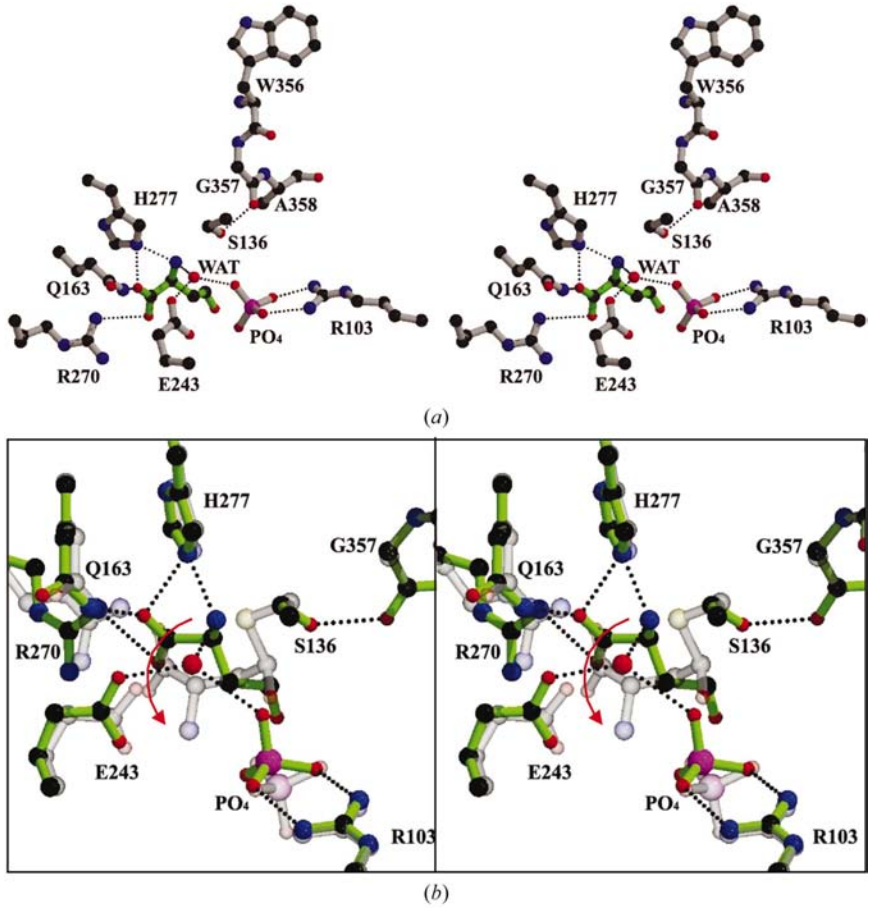

Figure 4
The active-site residues of the C136S ternary complex with ASA and phosphate. (*a*) Stereoview of the ternary complex showing the Ser136 hydroxyl group hydrogen bonding to the backbone carbonyl of Gly357, phosphate bound to Arg103 and ASA interacting with His277 and Arg270. (*b*) Overlay of the C136S ternary substrate complex of *hi*ASADH on the structure of the native enzyme with the covalently bound tetrahedral intermediate (gray bonds) (Blanco, Moore & Viola, 2003). A rotation of ASA (red arrow) is required to allow attack of Cys136 to form this tetrahedral intermediate. This figure was produced using *MOLSCRIPT* and *RASTER3D*.

His277. The acyl-enzyme intermediate can form from this enzyme–substrate complex only if the ASA amino group rotates away from His277 to allow nucleophilic attack by cysteine to take place at the aldehydic carbon. This rotation (red arrow in Fig. 4*b*) would allow the ASA α-carboxyl group to form the bidentate interaction with Arg270 that is seen in both the covalently bound tetrahedral intermediate and the SMCS-bound inhibitor structures of ASADH (Blanco, Moore, Kalabeeswaran *et al.*, 2003; Blanco, Moore & Viola, 2003). The α-amino group of the covalently bound intermediate also forms a new electrostatic interaction with the carboxyl of Glu243; the side chains of Arg270 and Glu243 must shift slightly to accommodate this rotation. The bound phosphate in the covalent intermediate structure shifts by 0.9 Å from its position in the C136S–ASA–P_i structure to match the movement by ASA. Thus, a precise rotation of ASA takes place during formation of the tetrahedral intermediate, putting the covalently bound acyl group in an ideal position for subsequent hydride transfer to NADP.

3.4. Role of the active-site acid–base catalyst

The proposed mechanism of ASADH (Blanco, Moore & Viola, 2003) suggests a function for His277 as an acid–base catalyst. Its role in facilitating nucleophilic attack by the cysteine thiolate anion on the substrate carbonyl carbon is supported kinetically by a four order-of-magnitude decrease in k_{cat} when this histidine is replaced by glutamine in the H274Q *ec*ASADH mutant (equivalent to *hi*ASADH His277) (James & Viola, unpublished observations). The published structures of ASADH from *E. coli* and *V. cholerae* (Blanco, Moore, Kalabeeswaran *et al.*, 2003; Hadfield *et al.*, 2001) are consistent with this proposed role for His277 by virtue of its close proximity to the catalytic thiol group of Cys136. This active-site histidine is also proposed to stabilize the hemithioacetal intermediate that is formed after attack of cysteine at the ASA carbonyl group (Blanco, Moore & Viola, 2003). The recently determined high-resolution structure of this tetrahedral intermediate places the N^{ε} atom of His277 within hydrogen-bonding distance of both the S atom of Cys136 and the substrate carboxyl group. This orientation would also stabilize the

trigonal planar thioester that forms after hydride transfer from the tetrahedral intermediate to NADP (Blanco, Moore & Viola, 2003). Interactions with the side-chain amide groups of Gln163 and Gln353 have been proposed to orient the imidazole ring and help to stabilize the positive charge that develops when this histidine is protonated (Hadfield *et al.*, 2001). These amide moieties are within hydrogen-bonding distance of the imidazole ring both in the native enzyme and in the C136S mutant, while the position of His277 remains unchanged in these structures.

The H277N mutant of *hi*ASADH was examined to assess the contributions of this acid–base group to catalysis. The refined model of H277N complexed with NADP and SMCS [$CH_3-S(=O)-CH_2-CH(NH_3^+)-COO^-$] shows that, as in the native enzyme, the inactivator covalently modifies both active sites of the dimer. Thus, the active-site cysteine nucleophile is still reactive enough to be modified by SMCS, even without the participation of histidine as a general base. Continuous density is observed extending from Cys136 in this structure, confirming the covalent attachment to the S^{γ} atom of SMCS (Fig. 5). However, similar to the *V. cholerae* NADP–SMCS complex (Blanco, Moore, Kalabeeswaran *et al.*, 2003), no density is observed for either the methyl group or the sulfoxide O atom that were originally part of SMCS. Clearly the reductive demethylation, involving the conversion of Cys136 to cystine that takes place once SMCS binds, does not require the participation of the histidine catalytic base.

The H277N mutant was co-crystallized with both SMCS and NADP. Well defined electron density is observed for the coenzyme in both subunits of one dimer (Fig. 5), but in only one subunit of the second dimer in the asymmetric unit. NADP binding has been proposed to be responsible for the conformational change between the 'open' apo form and the 'closed' holo form of the enzyme. A domain closure was observed in the *E. coli* ASADH structure upon binding of NADP, leading to a rotation of approximately 6° of the NADP-binding domain toward the dimerization domain in the

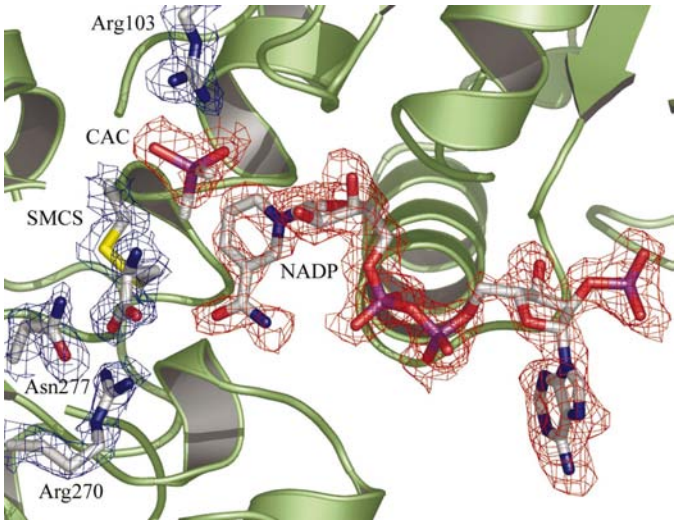

Figure 5
Active site of the *hi*ASADH H277N mutant. The active-site residues and the covalently attached cysteine derived from SMCS are shown as a $2F_o - F_c$ map (blue) contoured at 1.2σ, while bound NADP and cacodylate (CAC) are modeled into the $F_o - F_c$ electron-density map (red), contoured at 2σ. This figure was produced using *PyMOL*.

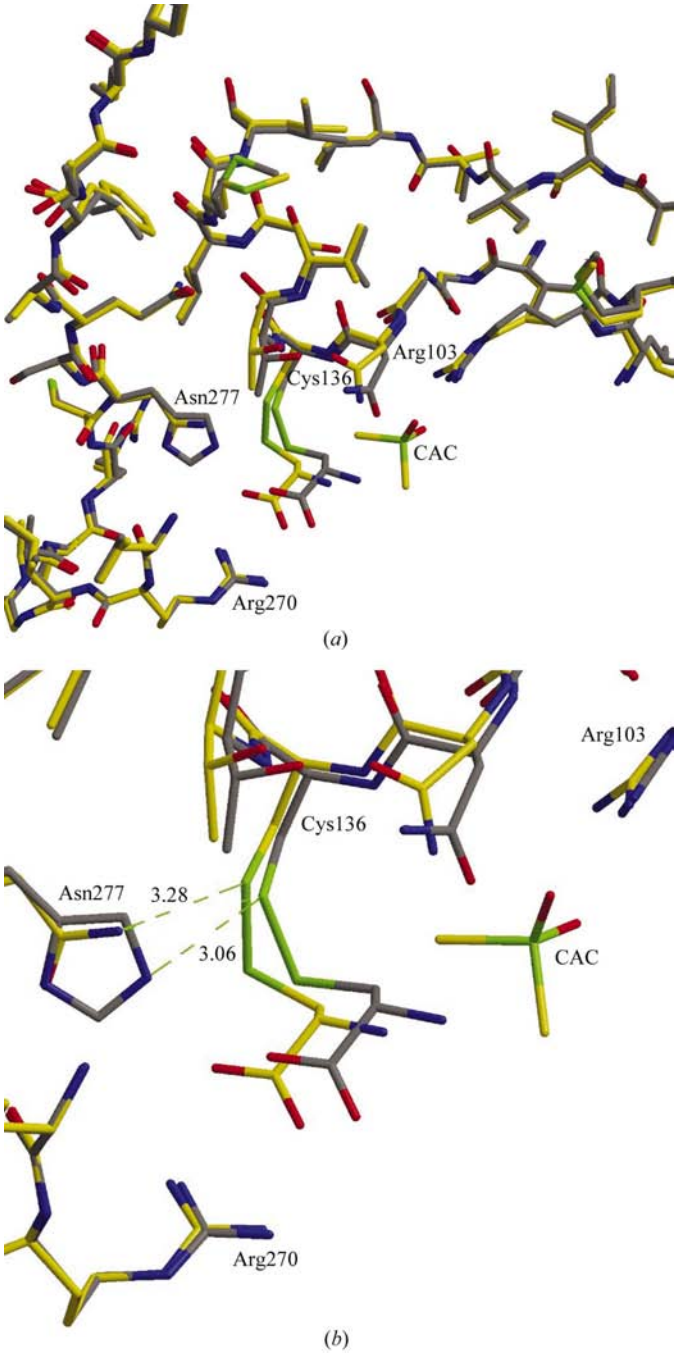

Figure 6
Superposition of the *hi*ASADH H277N mutant with bound SMCS on *vc*ASADH complexed with SMCS and NADP. Most of the side chains in this region have nearly identical positions between the *hi*ASADH structure (yellow bonds) and the *vc*ASADH structure (gray bonds) (Blanco, Moore & Viola, 2003). A molecule of the buffer cacodylate (CAC) is modeled into the phosphate-binding site in the *hi*ASADH structure. (*a*) Overview of the structure around the active-site region. (*b*) Expansion of the active site showing the movement of the covalently bonded cysteine derived from SMCS in response to the shorter side chain of Asn277. The coordinates were superimposed with *XtalView* and the figure was produced using *MOLSCRIPT* and *RASTER3D*.

presence of NADP (Hadfield *et al.*, 2001). However, the H277N structure presents both subunits in the closed conformation, even when NADP is absent from the binding site of one subunit. This observation provides further evidence to support the proposed communication between the binding events at the active sites in this dimer (Blanco, Moore, Kalabeeswaran *et al.*, 2003).

3.5. Repositioning of the enzyme-bound intermediate

The ASADHs from *H. influenzae* and *V. cholerae* have 69% overall sequence identity and 82% sequence similarity. Conservation of the three-dimensional structures between *hi*ASADH and *vc*ASADH is demonstrated by a least-squares superimposition of the structures using all of the backbone atoms, yielding an r.m.s. deviation of only 0.79 Å between the two structures. The side chains of the highly conserved active-site residues in these structures also superimpose at the same positions (Fig. 6*a*). The side chain of the introduced asparagine in H277N is positioned in the same orientation as that of the corresponding imidazole ring in *vc*ASADH. This places the amide N atom of Asn277 in the same relative location as the C^{δ} of the imidazole ring from *vc*ASADH (Fig. 6*a*) and is one bond removed from the position that was occupied by N^{ε} of imidazole. The decrease in side-chain length as a consequence of this mutation would result in an increase in the distance to S^{γ} and the carboxyl O atom and thus a disruption of the stabilization of the acyl-enzyme intermediate. Compensation for this shorter side chain requires the acyl intermediate as well as the covalently bound inactivator to change position in the active site. This new orientation in the H277N mutant places the S^{γ} of Cys136 less than 3.3 Å away from the amide N atom of Asn277 (Fig. 6*b*) and also moves the carboxyl O atom to within reasonable hydrogen-bonding distance. Despite this shift, the inhibitor carboxyl group still interacts in a bidentate manner with Arg270 (Fig. 6*b*), while the side-chain carboxyl group of Glu243 moves to maintain hydrogen-bonding distance with the amino group of SMCS.

The $k_{\rm cat}$ value for the H277N mutant is only 1% of that for the native enzyme (Table 3). This loss of activity could be caused by the absence of a suitable acid–base catalyst to aid in the ionization of Cys136. In that case, the pK of the active-site thiol would be elevated in the mutant relative to its value in the native enzyme. The rate of inactivation of *E. coli* ASADH by thiol reagents is pH-dependent; ionization of the active-site thiol with a pK value of 7.8 results in a fourfold increase in the inactivation rate (Karsten & Viola, 1991). Nucleophilic attack by a thiol with an elevated pK value in this mutant should become more efficient as the fraction of thiolate ion increases at higher pH; however, there is no increase in the activity of H277N at pH values up to 10.

The $K_{\rm m}$ values for ASA and phosphate in the H277N mutant remain essentially unchanged with respect to the native enzyme. This observation is corroborated by the identification of the same binding interactions in the mutant structure as are present in the native enzyme. Also, the rate of inactivation of H277N by SMCS is comparable to that of the native enzyme, so it is reasonable to assume that the Cys136 nucleophile in this mutant can also attack the ASA substrate with comparable efficiency. The decrease in overall enzyme efficiency in H277N must occur after this initial attack. The next step after hydride transfer is the attack by phosphate. After formation of the acyl intermediate in the H277N mutant, this new orientation moves the position of the carbonyl C atom further from the site of phosphate binding (Fig. 6*b*). It is reasonable to suggest that a similar increase in distance between phosphate and the bound intermediate would cause nucleophilic attack on the intermediate by phosphate to proceed with decreased efficiency. Certainly, other steps in the remainder of the catalytic cycle could also be affected. However, at the present time we have no data that would allow us to address how any subsequent steps may be altered by the removal of this catalytic group.

3.6. Identification of a new alternative substrate

Unexpectedly, the crystal structure of the H277N complex was found to have some extra unaccounted density in the phosphate-binding site and adjacent to Arg103. This density is not observed in any of the other ASADH structures that were crystallized in Tris buffer in the absence of phosphate. The H277N mutant was crystallized in the presence of sodium cacodylate (dimethylarsinate) as a buffer, an oxyanion that could potentially bind at the phosphate site. We have shown that an extensive group of oxyanions can interact with ASADH either as phosphate surrogates or as inhibitors (Kish & Viola, 1999), with the geometry and the charge density on the peripheral O atoms playing pivotal roles in binding. Two of the oxyanions studied, arsenate and vanadate, meet the charge and tetrahedral geometric requirements with sufficient fidelity to serve as alternative substrates for ASADH (Kish & Viola, 1999). A molecule of cacodylate added to the enzyme model at this position nicely accounts for this additional density (Fig. 5). To test the effect of cacodylate on the kinetics of the reaction this buffer was examined as a potential inhibitor of ASADH. Instead, cacodylate was found to be a weak alternative substrate, with a $k_{\rm cat}$ that is about 10% of that with phosphate and a $K_{\rm m}$ of 140 mM, nearly 100 times higher than that for phosphate. This higher $K_{\rm m}$ is not surprising since methyl groups have replaced two of the oxyanion O atoms that are important binding determinants. However, the interactions between the remaining O atoms and Arg103 are still sufficient to orient this group to serve as a nucleophile that can attack the acyl-enzyme intermediate and support the catalytic reaction.

4. Conclusions

These two active-site mutants each retain a low level of catalytic activity. The C136S mutant allows substrate binding, but formation of the covalently bound intermediate is slowed by a less efficient and misoriented nucleophile. In contrast, the H277N mutant forms the initial tetrahedral intermediate quite efficiently, but its subsequent breakdown is hindered by a shift

away from the bound phosphate nucleophile. In each case, small perturbations in the positioning of essential catalytic groups or reactive intermediates are shown to have dramatic effects on enzyme catalysis.

This work was supported by a grant from the National Science Foundation (MCB0196107). The authors wish to thank Dr Tim Mueser for helpful discussions on the analysis and refinement of the enzyme structures. Use of the Argonne National Laboratory at the Advanced Photon Source was supported by US Department of Energy, Office of Energy Research under Contract No. W-31-109-ENG-38. We thank the staff members at the Structural Biology Center (SBC) for their assistance with data collection.

References

Biellmann, J. F., Eid, P., Hirth, C. & Jornvall, H. (1980). *Eur. J. Biochem.* **104**, 53–58.
Blanco, J., Moore, R. A., Faehnle, C. R., Coe, D. M. & Viola, R. E. (2004). *Acta Cryst.* D**60**, 1388–1395.
Blanco, J., Moore, R. A., Kalabeeswaran, V. & Viola, R. E. (2003). *Protein Sci.* **12**, 27–33.
Blanco, J., Moore, R. A. & Viola, R. E. (2003). *Proc. Natl Acad. Sci. USA*, **100**, 12613–12617.
Bradford, M. (1976). *Anal. Biochem.* **72**, 248–253.
Brünger, A. T., Adams, P. D., Clore, G. M., DeLano, W. L., Gros, P., Grosse-Kunstleve, R. W., Jiang, J.-S., Kuszewski, J., Nilges, M., Pannu, N. S., Read, R. J., Rice, L. M., Simonson, T. & Warren, G. L. (1998). *Acta Cryst.* D**54**, 905–921.
Cleland, W. W. (1967). *Adv. Enzymol.* **29**, 1–32.
Cohen, G. N. (1983). *Amino Acids: Biosynthesis and Genetic Regulation*, edited by K. M. Herrmann & R. L. Somerville, pp. 147–171. Reading, MA, USA: Addison-Wesley.
Cox, R. J., Hadfield, A. T. & Mayo-Martin, M. B. (2001). *Chem. Commun.* **18**, 1710–1711.
Cox, R. J., Sutherland, A. & Vederas, J. C. (2000). *Bioorg. Med. Chem.* **8**, 843–871.
Fleischmann, R. D. *et al.* (1995). *Science*, **269**, 496–512.
Galan, J. E., Nakayama, K. & Curtiss, R. (1990). *Gene*, **94**, 29–35.
Hadfield, A. T., Kryger, G., Ouyang, J., Petsko, G. A., Ringe, D. & Viola, R. E. (1999). *J. Mol. Biol.* **289**, 991–1002.
Hadfield, A. T., Shammas, C., Kryger, G., Ringe, D., Petsko, G. A., Ouyang, J. & Viola, R. E. (2001). *Biochemistry*, **40**, 14475–14483.
Harb, O. S. & Kwaik, Y. A. (1998). *Infect. Immun.* **66**, 1898–1903.
Harris, J. I. & Waters, M. J. (1976). *The Enzymes*, edited by P. D. Boyer, pp. 1–50. New York: Academic Press.
Holland, M. J. & Westhead, E. W. (1973). *Biochemistry*, **12**, 2264–2270.
Kang, H. Y., Srinivasan, J. & Curtiss, R. (2002). *Infect. Immun.* **70**, 1739–1749.
Karsten, W. E. & Viola, R. E. (1991). *Biochim. Biophys. Acta*, **1077**, 209–219.
Karsten, W. E. & Viola, R. E. (1992). *Biochim. Biophys. Acta*, **1121**, 234–238.
Kish, M. M. & Viola, R. E. (1999). *Inorg. Chem.* **38**, 818–820.
Krimsky, I. & Racker, E. (1955). *Science*, **122**, 319–323.
McRee, D. E. (1999). *J. Struct. Biol.* **125**, 156–165.
Moore, R. A., Bocik, W. E. & Viola, R. E. (2002). *Protein Expr. Purif.* **25**, 189–194.
Moras, D., Olsen, K. W., Sabesan, M. N., Buehner, M., Ford, G. C. & Rossmann, G. M. (1975). *J. Biol. Chem.* **250**, 9137–9162.
Nakayama, K., Kelly, S. M. & Curtiss, R. (1988). *Biotechnology*, **6**, 693–697.
Otwinowski, Z. & Minor, W. (1997). *Methods Enzymol.* **276**, 307–326.
Ouyang, J. & Viola, R. E. (1995). *Biochemistry*, **34**, 6394–6399.
Patte, J. C. (1983). *Amino Acids: Biosynthesis and Genetic Regulation*, edited by K. M. Herrmann & R. L. Somerville, pp. 213–228. Reading, MA, USA: Addison-Wesley.
Viola, R. E. (2001). *Acc. Chem. Res.* **34**, 339–349.
Yun, M., Park, C., Kim, J. & Park, H. (2000). *Biochemistry*, **39**, 10702–10710.